UNIVERSIDAD DE CONCEPCIÓN

Centro de Investigación en
Ingeniería Matemática (CI^{2}MA)

An entropy stable and well-balanced scheme for an augmented blood flow model with variable geometrical and mechanical properties

Raimund Bürger, Andrés Guerra,
Carlos A. Vega

PREPRINT 2025-03

SERIE DE PRE-PUBLICACIONES

AN ENTROPY STABLE AND WELL-BALANCED SCHEME FOR AN AUGMENTED BLOOD FLOW MODEL WITH VARIABLE GEOMETRICAL AND MECHANICAL PROPERTIES

RAIMUND BÜRGER[A], ANDRÉS GUERRA[B], AND CARLOS A. VEGA[B,*]

Abstract. The flow of blood through a vessel can be described by a hyperbolic system of balance equations for the cross-sectional area and averaged velocity as functions of axial spatial position and time. The variable arterial wall rigidity and the equilibrium cross-sectional area are incorporated within the so-called tube law that gives rise to an internal pressure term. This system can be written as a conservative hyperbolic system for five unknowns. An entropy stable scheme for this augmented one-dimensional blood flow model is developed based on entropy conservative numerical flux. It is proved that the proposed scheme is well-balanced in the sense that it preserves both trivial (zero velocity) and non-trivial (non-zero velocity) steady-state solutions. Several demanding numerical tests show that the scheme can handle various kinds of shocks and preserves stationary solutions when geometrical and mechanical properties of the vessel are variable.

1. Introduction

1.1. **Scope.** We are interested in numerical schemes for a one-dimensional model of the flow of blood through an artery. The model can be derived by averaging the incompressible three-dimensional Navier-Stokes equations over the cross section of the artery, under two assumptions usually held in most applications, namely an axisymmetric velocity profile and large wavelengths compared with the radius of the vessel [12]. The resulting one-dimensional inviscid system of partial differential equations (PDEs) for the blood flow in terms of the area $A = A(x,t)$ and the velocity $U = U(x,t)$ (in short, "(A,U) model") can be written as [31]

$$\partial_t A + \partial_x(AU) = 0, \quad \partial_t U + \partial_x \left(\frac{1}{2}U^2\right) + \frac{1}{\rho}P_x = 0, \tag{1.1}$$

where $A(x,t) = \pi R^2(x,t)$ is the cross-sectional area of the vessel at axial spatial position x and time t, where $R(x,t)$ is the radius, $U(x,t)$ is the mean blood velocity in the axial direction, ρ is the blood density that is assumed to be constant, and $P = P(x,t)$ is the internal pressure. We consider the blood flow model with flat velocity profile, i.e., the axial component of the velocity is assumed constant in the radial direction due to the inviscid flow assumption. The system (1.1) is closed by a constitutive equation relating pressure and cross-sectional area. Here, we employ the so-called tube law, namely [35]

$$P(x,t) = P_{\mathrm{e}}(x) + K(x)\phi\big(A(x,t), A_0(x)\big), \tag{1.2}$$

Date: January 13, 2025.

Key words and phrases. Augmented blood flow model; vessel with variable properties; well-balanced scheme; entropy stable scheme.

*Corresponding author.

[A]CI^{2}MA and Departamento de Ingeniería Matemática, Facultad de Ciencias Físicas y Matemáticas, Universidad de Concepción, Casilla 160-C, Concepción, Chile. E-Mail: rburger@ing-mat.udec.cl.

[B]Departamento de Matemáticas y Estadística, Universidad del Norte, Km 5 via Puerto Colombia, Barranquilla, Colombia. E-Mail: aguerraj@uninorte.edu.co, cvega@uninorte.edu.co.

where $P_\mathrm{e} = P_\mathrm{e}(x)$ denotes the external pressure, A_0 is the equilibrium cross-sectional area (i.e. the cross-sectional area when $P = P_\mathrm{e}$), $K(x)$ is the wall stiffness coefficient, and the function ϕ is defined by

$$\phi(A, A_0) \coloneqq (A/A_0)^m - (A/A_0)^n. \tag{1.3}$$

The parameters m and n depend on the vessel type. Typical values for collapsible tubes, such as veins, are $m = 10$ and $n = -1.5$; for arteries, $m = 0.5$ and $n = 0$.

It is the purpose of this work is to develop high-order, entropy-stable and well-balanced scheme for an augmented reformulation of the (A, U) one-dimensional blood flow model (1.1)–(1.3), supplied with initial and boundary conditions. This augmented formulation treats the variable parameters, namely the arterial wall rigidity $K(x)$, the cross-sectional area at rest $A_0(x)$ and the external pressure $P_\mathrm{e}(x)$ as unknowns. The proposed numerical scheme preserves non-trivial stationary solutions and captures the correct solutions even in the case of discontinuous variation of the geometrical and mechanical properties of the vessels. Augmented formulations of the blood flow models with varying properties have been considered in [20] and [26] but these approximations are based on writing the governing equations in terms of conserved variables, that is, the cross-sectional area A and the flow rate $Q = AU$. The augmented system can be written in conservation-law form. This property avoids the discretization of source terms and facilitates the construction of an explicit entropy conservative flux along with the dissipation operator. It is, however, unnecessary to calculate all entries of the corresponding scaling matrix.

1.2. **Related work.** The origin of quantitative studies in the cardiovascular system begins with Leonhard Euler (1707–1783). In his essay *Principia pro motu sanguinis per arterias determinando* (On the flow of blood in the arteries) [8], Euler proposed the one-dimensional equations of conservation of mass and momentum in a elastic tube, where the cross-sectional area, mean velocity and pressure were the unknown variables. Nowadays, one-dimensional (1D) blood flow models are a very active area of research, due to their ability to capture physiological waveforms [1, 3, 21, 31]. These models can provide useful information to diagnose some pathologies, such as stenoses or aneurysms, and help prevent cardiovascular incidents [22, 25]. On the other hand, 1D models can be coupled to more complex 3D models to handle boundary conditions, obtain more accurate information and reduce the cost of simulations [11, 25]. Such models are also useful for modeling blood flow in a network of connected vessels with variable properties [13, 20, 27], particularly for modelling studies based on tree structure for both arterial and venous circulation [22, 23]. An alternative approach of avoiding the complexity of three-dimensional models consists in describing the flow of blood through vessels in two dimensional, an axial plus a radial one, as is proposed in [29].

Due to non-linearity of 1D blood flow models, it is in general not possible to find exact solutions. However, some progress in this direction has been made for particular cases: Spilimbergo et al. [32] and Toro and Siviglia [35] obtained exact solutions of the Riemann problem for the inviscid model in the “star region,” in [30] Riemann solutions in the velocity-area plane were constructed by using the global entropy condition to select the physically relevant solution, and in [36] solutions of the linearized model with friction and diffusion terms are obtained to be compared with clinical observations and numerical solutions. The literature on numerical methods for approximating solutions of 1D blood flow models is vast. Recently many researchers have been focusing on well-balanced schemes, that is, schemes that can preserve certain steady state solutions. Strategies used to obtain this crucial property include central-upwind schemes by using flux globalization [6], finite-volume schemes based on hydrostatic reconstruction [7, 15, 17], the ADER (Arbitrary high-order DERivative) framework [19, 20], discontinuous Galerkin methods [4, 17, 28], and finite difference methods [5].

1.3. **Outline of the paper.** The remainder of this paper is organized as follows. Section 2 gives a concise presentation of the augmented model including the entropy pair which is a key ingredient to construct entropy stable schemes. Section 3 contains the main contributions i.e., to derive an explicit entropy conservative flux for the model using the framework proposed in [9]. Then a diffusion operator is added to obtain an entropy stable scheme. The remainder of this section will be devoted to the proof of the well-balanced property. Numerical tests are presented in Section 4 which demonstrate that the constructed schemes preserve stationary solutions and capture shocks correctly. Finally, some conclusions are drawn in Section 5.

2. Analysis of the model

2.1. **Augmented formulation.** The augmented formulation of system (1.1) regards the variable parameters $K(x)$, $A_0(x)$, and $P_\mathrm{e}(x)$ as new unknowns. Since these three quantities are constant in time, their temporal derivatives can be added to the system (1.1). Thus, the augmented (A, U) system of conservation laws

$$\partial_t \boldsymbol{u} + \partial_x \boldsymbol{f}(\boldsymbol{u}) = \boldsymbol{0} \tag{2.1}$$

is obtained, where

$$\boldsymbol{u} \coloneqq \begin{pmatrix} A \\ U \\ K \\ A_0 \\ P_\mathrm{e} \end{pmatrix} \quad \text{and} \quad \boldsymbol{f}(\boldsymbol{u}) \coloneqq \begin{pmatrix} AU \\ U^2/2 + (P_\mathrm{e} + K\phi(A, A_0))/\rho \\ 0 \\ 0 \\ 0 \end{pmatrix} \tag{2.2}$$

are the vector of unknowns and the flux density vector, respectively. In quasi-linear form the system (2.1) reads

$$\partial_t \boldsymbol{u} + \boldsymbol{J}\partial_x \boldsymbol{u} = \boldsymbol{0}, \tag{2.3}$$

where the Jacobian matrix of the flux function is given by

$$\boldsymbol{J} \coloneqq \boldsymbol{f}_{\boldsymbol{u}} = \begin{bmatrix} U & A & 0 & 0 & 0 \\ c^2/A & U & \phi/\rho & K\phi_{A_0}/\rho & 1/\rho \\ 0 & 0 & 0 & 0 & 0 \\ 0 & 0 & 0 & 0 & 0 \\ 0 & 0 & 0 & 0 & 0 \end{bmatrix},$$

where

$$c \coloneqq \sqrt{\frac{KA}{\rho}\phi_A} = \sqrt{\frac{K}{\rho}(ma^m - na^n)}, \quad a \coloneqq A/A_0,$$

is the Moens-Korteweg wave speed which is real for the values of m and n given above, and the eigenvalues of $\boldsymbol{f}_{\boldsymbol{u}}$ are

$$\lambda_1 = U - c, \qquad \lambda_2 = \lambda_3 = \lambda_4 = 0, \qquad \lambda_5 = U + c. \tag{2.4}$$

2.2. **Hyperbolicity and Riemann invariants.** The hyperbolicity of the system (2.3) is characterized by the Shapiro number

$$S_\mathrm{h} \coloneqq |U|/c. \tag{2.5}$$

The Shapiro number is the analogue of the Froude number for shallow water equations and depending on its value two flow regimes are distinguished: subcritical and supercritical. For $S_\mathrm{h} \neq 1$ a complete set of independent right eigenvectors of $\boldsymbol{J}$ corresponding to eigenvalues (2.4) is given by

$$\boldsymbol{r}_1 = \begin{pmatrix} -1 \\ c/A \\ 0 \\ 0 \\ 0 \end{pmatrix}, \ \boldsymbol{r}_2 = \begin{pmatrix} 1 \\ -U/A \\ 0 \\ 0 \\ \rho(U^2 - c^2)/A \end{pmatrix}, \ \boldsymbol{r}_3 = \begin{pmatrix} 0 \\ 0 \\ 1 \\ 0 \\ -\phi \end{pmatrix}, \quad \boldsymbol{r}_4 = \begin{pmatrix} 0 \\ 0 \\ 0 \\ 1 \\ -K\phi_{A_0} \end{pmatrix}, \ \boldsymbol{r}_5 = \begin{pmatrix} 1 \\ c/A \\ 0 \\ 0 \\ 0 \end{pmatrix}. \quad (2.6)$$

Consequently, if $S_\mathrm{h} < 1$ (subcritical flow) or $S_\mathrm{h} > 1$ (supercritical flow) the system is hyperbolic (all eigenvalues are real and the system of eigenvectors is complete), but not strictly hyperbolic (since the eigenvalues are not pairwise distinct). In the case $S_\mathrm{h} = 1$ (critical flow) the system loses its hyperbolicity (the set of eigenvectors is no longer complete), leading to resonance phenomena. For $S_\mathrm{h} \neq 1$ we can write $\boldsymbol{J} = \boldsymbol{R}\boldsymbol{\Lambda}\boldsymbol{R}^\mathrm{T}$, where the columns of $\boldsymbol{R}$ are eigenvectors given by (2.6) and $\boldsymbol{\Lambda}$ is a diagonal matrix containing the eigenvalues of $\boldsymbol{J}$.

On the other hand, it is obvious that the second, third and fourth characteristic fields are linearly degenerate. The Riemann invariants associated with these fields are

$$\Gamma_1^\mathrm{LD} = AU, \quad \Gamma_2^\mathrm{LD} = \frac{1}{2}U^2 + \frac{1}{\rho}(P_\mathrm{e} + K\phi).$$

For the first and fifth characteristic fields, an easy computation shows that

$$\nabla\lambda_1 \cdot \boldsymbol{r}_1 = \nabla\lambda_5 \cdot \boldsymbol{r}_5 = \frac{\partial c}{\partial A} + \frac{c}{A} = \frac{\sqrt{K}(m(m+2)a^m - n(n+2)a^n)}{2A\sqrt{\rho(ma^m - na^n)}}.$$

Therefore the first and fifth characteristic fields are genuinely non-linear provided that

$$m(m+2)a^m \neq n(n+2)a^n.$$

This inequality holds for the aforementioned values of m and n for veins and arteries. The Riemann invariants associated with the genuinely non-linear fields are

$$\Gamma_1 = U + \int \frac{c(A)}{A}\,\mathrm{d}A, \quad \Gamma_2 = U - \int \frac{c(A)}{A}\,\mathrm{d}A.$$

2.3. **Steady-state solutions.** The augmented system (2.1) admits the non-trivial steady-state solution

$$AU = C_1 \quad \text{and} \quad E := \frac{U^2}{2} + \frac{1}{\rho}\big(P_\mathrm{e} + K\phi(A, A_0)\big) = C_2, \quad (2.7)$$

where C_1 and C_2 are constants. The quantity E is known as the *energy discharge*. This steady state is known as the *living-man equilibrium*. In particular, the *steady state at rest*, or *man-at-eternal-rest* equilibrium (by analogy to the *lake at rest* in the shallow water equations) is given by

$$U = 0 \quad \text{and} \quad P_\mathrm{e} + K\phi(A, A_0) = C_3 \quad (2.8)$$

for a constant C_3.

2.4. **Entropy pair.** We now turn to the existence of a entropy pair for the system (2.3) [11], that is a pair (η, G) of functions where the entropy $\eta = \eta(\boldsymbol{u})$ is a convex function and $G = G(\boldsymbol{u})$ satisfies $G_{\boldsymbol{u}} = \eta_{\boldsymbol{u}} \boldsymbol{f}_{\boldsymbol{u}}$, where we write $G_{\boldsymbol{u}} \coloneqq \nabla G(\boldsymbol{u})$ and $\eta_{\boldsymbol{u}} \coloneqq \nabla \eta(\boldsymbol{u})$. The existence of such an entropy pair is essential to select the physically correct one among all weak solutions of the system. On the other hand, it is well known [18] that a system of conservation laws equipped with and entropy pair is symmetrizable by using the change of variables $\boldsymbol{u} \to \boldsymbol{v}$ where $\boldsymbol{v} = (\eta_{\boldsymbol{u}})^{\mathrm{T}}$ denotes the entropy variables. More precisely, if we set $\boldsymbol{u} = \boldsymbol{u}(\boldsymbol{v})$ then the quasilinear form (2.3) becomes

$$\boldsymbol{u}_{\boldsymbol{v}} \partial_t \boldsymbol{v} + \boldsymbol{f}_{\boldsymbol{v}} \partial_x \boldsymbol{v} = \boldsymbol{0},$$

where $\boldsymbol{f}_{\boldsymbol{v}}$ is symmetric and $\boldsymbol{u}_{\boldsymbol{v}}$ is symmetric positive definite. The fact that the entropy variables symmetrize the system will be crucial in constructing the diffusion operator to be discussed in the next section.

Lemma 2.1. *If $S_{\mathrm{h}} < 1$, the pair of functions (η, G) given by*

$$\eta(\boldsymbol{u}) \coloneqq \frac{P_{\mathrm{e}} A}{\rho} + \frac{AU^2}{2} + \frac{K\Phi(A, A_0)}{\rho} + h_1(K) + h_2(A_0) + h_3(P_{\mathrm{e}}) \quad \text{and}$$
$$G(\boldsymbol{u}) \coloneqq \frac{P_{\mathrm{e}} AU}{\rho} + \frac{AU^3}{2} + \frac{K\Phi(A, A_0)AU}{\rho}$$

is an entropy pair for (2.3). Here, h_1, h_2 and h_3 can be any smooth functions and

$$\Phi(A, A_0) = \int^A \phi(\tau, A_0)\,\mathrm{d}\tau = A_0 \left(\frac{(A/A_0)^{m+1}}{m+1} - \frac{(A/A_0)^{n+1}}{n+1} \right) = A_0 \left(\frac{a^{m+1}}{m+1} - \frac{a^{n+1}}{n+1} \right),$$

where $a = A/A_0$.

Proof. Let us first prove that $\partial_t \eta(\boldsymbol{u}) + \partial_x G(\boldsymbol{u}) = 0$ for a smooth solution $\boldsymbol{u}$ of system (2.3). Taking into account that the first and second component of the gradient of η are the second and first component of the flux function respectively, and using (2.1) we get

$$\begin{aligned}
\partial_t \eta(\boldsymbol{u}) + \partial_x G(\boldsymbol{u}) &= \nabla \eta \partial_t \boldsymbol{u} + \partial_x G(\boldsymbol{u}) \\
&= \left(\frac{P_{\mathrm{e}}}{\rho} + \frac{U^2}{2} + \frac{K\phi}{\rho} \right) \partial_t A + AU \partial_t U + \partial_x G(\boldsymbol{u}) \\
&= \left(\frac{P_{\mathrm{e}}}{\rho} + \frac{U^2}{2} + \frac{K\phi}{\rho} \right) \partial_x(-AU) - AU \partial_x \left(\frac{P_{\mathrm{e}}}{\rho} + \frac{U^2}{2} + \frac{K\phi}{\rho} \right) + \partial_x G(\boldsymbol{u}) \\
&= -\partial_x \left(AU \left(\frac{P_{\mathrm{e}}}{\rho} + \frac{U^2}{2} + \frac{K\phi}{\rho} \right) \right) + \partial_x G(\boldsymbol{u}) = -\partial_x G(\boldsymbol{u}) + \partial_x G(\boldsymbol{u}) = 0.
\end{aligned}$$

It remains to prove that η is convex. The leading principal minors of the Hessian matrix $\eta_{\boldsymbol{u}\boldsymbol{u}}$ are

$$\begin{aligned}
M_1 &= c^2/A, \qquad M_2 = c^2 - U^2, \qquad M_3 = h_1''(K)(c^2 - U^2) - A\phi^2/\rho^2, \\
M_4 &= \left(h_1''(K) \left(\frac{K\Phi_{A_0A_0}}{\rho} + h_2''(A_0) \right) - \frac{\Phi_{A_0}}{\rho} \right) (c^2 - U^2) + \frac{2AK\phi\Phi_{A_0}\phi_{A_0}}{\rho^3} \\
&\quad - \frac{AK^2 h_1''(K)\phi_{A_0}^2}{\rho^2} - \frac{A\phi^2}{\rho^2} \left(\frac{K\Phi_{A_0A_0}}{\rho} + h_2''(A_0) \right), \\
M_5 &= -\frac{A}{\rho^2} \left(h_1''(K) \left(\frac{K\Phi_{A_0A_0}}{\rho} + h_2''(A_0) \right) - \frac{\Phi_{A_0}}{\rho} \right) + M_4 h_3(P_{\mathrm{e}}).
\end{aligned}$$

Since h_1, h_2, and h_3 are adjustable, $\eta_{\boldsymbol{u}\boldsymbol{u}}$ is positive definite if $c^2 - U^2 > 0$ or equivalently, $S_{\mathrm{h}} < 1$. ◻

3. Numerical schemes

3.1. **Entropy stable and entropy conservative semi-discrete schemes.** A semi-discrete finite volume scheme for (2.1) on a uniform spatial mesh with nodes $x_j = j\Delta x$, $j \in \mathbb{Z}$ is given by

$$\frac{\mathrm{d}\boldsymbol{u}_j(t)}{\mathrm{d}t} = -\frac{1}{\Delta x}\left(\boldsymbol{F}_{j+1/2} - \boldsymbol{F}_{j-1/2}\right), \quad j \in \mathbb{Z}, \tag{3.1}$$

where $\boldsymbol{u}_j(t)$ is the cell average on $I_j = [x_{j-1/2}, x_{j+1/2})$ and $\boldsymbol{F}_{j+1/2}$ is a consistent numerical flux associated with $x_{j+1/2}$. The scheme (3.1) is called *entropy stable* with respect to the entropy pair (η, G) if it satisfies a discrete entropy inequality

$$\frac{\mathrm{d}}{\mathrm{d}t}\eta\bigl(\boldsymbol{u}_j(t)\bigr) + \frac{1}{\Delta x}\bigl(\tilde{G}_{j+1/2} - \tilde{G}_{j-1/2}\bigr) \leq 0 \tag{3.2}$$

for some numerical entropy flux $\tilde{G}_{j+1/2}$ consistent with the entropy flux G. If equality holds in (3.2), then the scheme (3.1) is called *entropy conservative*.

3.2. **Second-order entropy conservative scheme.** We are interested in finding an entropy stable scheme for the 1D blood flow model. For this purpose, we first recall a basic result to design entropy conservative numerical fluxes.

Theorem 3.1 (Tadmor [33])**.** *The scheme (3.1) is second-order accurate and entropy conservative if the numerical flux $\tilde{\boldsymbol{F}}_{j+1/2}$ is consistent and satisfies*

$$\bigl\langle [\![\boldsymbol{v}]\!]_{j+1/2}, \tilde{\boldsymbol{F}}_{j+1/2}\bigr\rangle = [\![\psi]\!]_{j+1/2} \quad \text{for all } j \in \mathbb{Z}, \tag{3.3}$$

where $[\![\cdot]\!]_{j+1/2}$ represents the jump of a quantity across the interface at $x_{j+1/2}$ and ψ is the entropy potential defined as

$$\psi(\boldsymbol{u}) \coloneqq \bigl\langle \boldsymbol{v}, \boldsymbol{f}(\boldsymbol{u})\bigr\rangle - G(\boldsymbol{u}).$$

Using this key result we may construct an entropy conservative flux for the model(2.1). Let us introduce the notation

$$\{\!\{a\}\!\}_{j+1/2} \coloneqq \frac{1}{2}(a_{j+1} + a_j).$$

It is evident that $\{\!\{a\}\!\}_{j+1/2} = a$ when $a_{j+1} = a_j = a$.

Theorem 3.2. *For the augmented (A, U) blood flow model (2.1) the numerical flux*

$$\tilde{\boldsymbol{F}}_{j+1/2} \coloneqq \tilde{\boldsymbol{F}}(\boldsymbol{u}_j, \boldsymbol{u}_{j+1}) \coloneqq \begin{pmatrix} \{\!\{f_1\}\!\}_{j+1/2} \\ \{\!\{f_2\}\!\}_{j+1/2} \\ 0 \\ 0 \\ 0 \end{pmatrix} = \begin{pmatrix} \{\!\{AU\}\!\}_{j+1/2} \\ \{\!\{P_\mathrm{e}/\rho + U^2/2 + K\phi/\rho\}\!\}_{j+1/2} \\ 0 \\ 0 \\ 0 \end{pmatrix} \tag{3.4}$$

is entropy conservative and consistent with the flux density vector $\boldsymbol{f}(\boldsymbol{u})$ defined in (2.2). Here $f_1(\boldsymbol{u})$ and $f_2(\boldsymbol{u})$ are the first two components of $\boldsymbol{f}(\boldsymbol{u})$.

Proof. We first compute the entropy variables and entropy potential for the augmented (A, U) blood flow model:

$$\begin{aligned} \boldsymbol{v} = \bigl(\eta_{\boldsymbol{u}}(\boldsymbol{u})\bigr)^{\mathrm{T}} &= \left(\frac{P_\mathrm{e}}{\rho} + \frac{U^2}{2} + \frac{K\phi}{\rho}, AU, \frac{\Phi}{\rho} + h_1'(K), \frac{K\Phi_{A_0}}{\rho} + h_2'(A_0), \frac{A}{\rho} + h_3'(P_\mathrm{e})\right)^{\mathrm{T}} \\ &= \left(f_2(\boldsymbol{u}), f_1(\boldsymbol{u}), \frac{\Phi}{\rho} + h_1'(K), \frac{K\Phi_{A_0}}{\rho} + h_2'(A_0), \frac{A}{\rho} + h_3'(P_\mathrm{e})\right)^{\mathrm{T}} \end{aligned} \tag{3.5}$$

and

$$\psi(\boldsymbol{u}) = \boldsymbol{v}^{\mathrm{T}}\boldsymbol{f} - G = \left(\frac{P_{\mathrm{e}}}{\rho} + \frac{U^2}{2} + \frac{K\phi}{\rho}\right) AU = f_2(\boldsymbol{u}) f_1(\boldsymbol{u}). \tag{3.6}$$

Taking

$$\tilde{\boldsymbol{F}}_{j+1/2} = \big(\tilde{F}^{(1)}_{j+1/2}, \tilde{F}^{(2)}_{j+1/2}, 0, 0, 0\big)^{\mathrm{T}}$$

and inserting (3.5) and (3.6) into (3.3) yields

$$[\![f_2]\!]_{j+1/2} \tilde{F}^{(1)}_{j+1/2} + [\![f_1]\!]_{j+1/2} \tilde{F}^{(2)}_{j+1/2} = [\![f_2 f_1]\!]_{j+1/2}. \tag{3.7}$$

We next use the identity

$$[\![ab]\!]_{j+1/2} = \{\!\{ a \}\!\}_{j+1/2} [\![b]\!]_{j+1/2} + \{\!\{ b \}\!\}_{j+1/2} [\![a]\!]_{j+1/2}$$

in the right-hand side of (3.7) to obtain

$$[\![f_2]\!]_{j+1/2} \tilde{F}^{(1)}_{j+1/2} + [\![f_1]\!]_{j+1/2} \tilde{F}^{(2)}_{j+1/2} = \{\!\{ f_2 \}\!\}_{j+1/2} [\![f_1]\!]_{j+1/2} + \{\!\{ f_1 \}\!\}_{j+1/2} [\![f_2]\!]_{j+1/2}.$$

Equating the coefficients of the same jump terms gives

$$\tilde{F}^{(1)}_{j+1/2} = \{\!\{ f_1 \}\!\}_{j+1/2} \quad \text{and} \quad \tilde{F}^{(2)}_{j+1/2} = \{\!\{ f_2 \}\!\}_{j+1/2},$$

which in turn gives (3.4) considering that the last three components of the numerical flux are null. It remain to prove consistency. If $\boldsymbol{u}_j = \boldsymbol{u}_{j+1} = \boldsymbol{u}$, then $\{\!\{ f_1 \}\!\}_{j+1/2} = f_1(\boldsymbol{u})$ and $\{\!\{ f_2 \}\!\}_{j+1/2} = f_2(\boldsymbol{u})$. Thus $\tilde{\boldsymbol{F}}(\boldsymbol{u}, \boldsymbol{u}) = \boldsymbol{f}(\boldsymbol{u})$, which completes the proof. □

3.3. **Higher-order entropy conservative scheme.** According to Theorem 3.1 the numerical flux (3.4) is only second-order accurate. To construct $2p$-th ($p \in \mathbb{N}$) order accurate entropy conservative fluxes, LeFloch et al. [16] proposed the formula

$$\tilde{\boldsymbol{F}}^{2p}_{j+1/2} \coloneqq \sum_{i=1}^{p} \gamma_i^p \sum_{s=0}^{i-1} \tilde{\boldsymbol{F}}(\boldsymbol{u}_{j-s}, \boldsymbol{u}_{j-s+i}), \tag{3.8}$$

where $\tilde{\boldsymbol{F}}(\cdot,\cdot)$ are two-point entropy conservative fluxes satisfying (3.3) and the coefficients γ_i^p, $i = 1, \dots, p$ solve the linear equations

$$\sum_{i=1}^{p} i \gamma_i^p = 1, \qquad \sum_{i=1}^{p} i^{2s-1} \gamma_i^p = 1 \quad (s = 2, \dots, p).$$

For instance, the fourth- and sixth-order entropy conservative fluxes corresponding to $p = 2$ and $p = 3$ are explicitly given as

$$\begin{aligned}
\tilde{\boldsymbol{F}}^{4}_{j+1/2} &= \frac{4}{3}\tilde{\boldsymbol{F}}(\boldsymbol{u}_j, \boldsymbol{u}_{j+1}) - \frac{1}{6}\big(\tilde{\boldsymbol{F}}(\boldsymbol{u}_{j-1}, \boldsymbol{u}_{j+1}) + \tilde{\boldsymbol{F}}(\boldsymbol{u}_j, \boldsymbol{u}_{j+2})\big), \\
\tilde{\boldsymbol{F}}^{6}_{j+1/2} &= \frac{3}{2}\tilde{\boldsymbol{F}}(\boldsymbol{u}_j, \boldsymbol{u}_{j+1}) - \frac{3}{10}\big(\tilde{\boldsymbol{F}}(\boldsymbol{u}_{j-1}, \boldsymbol{u}_{j+1}) + \tilde{\boldsymbol{F}}(\boldsymbol{u}_j, \boldsymbol{u}_{j+2})\big) \\
&\quad + \frac{1}{30}\big(\tilde{\boldsymbol{F}}(\boldsymbol{u}_{j-1}, \boldsymbol{u}_{j+1}) + \tilde{\boldsymbol{F}}(\boldsymbol{u}_{j-1}, \boldsymbol{u}_{j+2}) + \tilde{\boldsymbol{F}}(\boldsymbol{u}_j, \boldsymbol{u}_{j+3})\big).
\end{aligned}$$

3.4. **Diffusion matrix.** So far we have constructed a $2p$-th order entropy conservative flux for the (A, U) blood flow model. A k-th order entropy stable scheme is obtained by adding a diffusion operator to the entropy conservative flux (3.4), (3.8), which yields

$$\boldsymbol{F}^k_{j+1/2} = \tilde{\boldsymbol{F}}^{2p}_{j+1/2} - \frac{1}{2}\boldsymbol{D}_{j+1/2}\langle\langle \boldsymbol{v}\rangle\rangle_{j+1/2} \tag{3.9}$$

(see [9, Lemma 3.2]), where

$$\langle\langle \boldsymbol{v}\rangle\rangle_{j+1/2} := \boldsymbol{v}^-_{j+1/2} - \boldsymbol{v}^+_{j+1/2}$$

is the difference in the k-th order reconstructed states and $\boldsymbol{D}_{j+1/2}$ is a diffusion matrix of the form

$$\boldsymbol{D}_{j+1/2} = \tilde{\boldsymbol{R}}_{j+1/2}\tilde{\boldsymbol{\Lambda}}_{j+1/2}\tilde{\boldsymbol{R}}^{\mathrm{T}}_{j+1/2}.$$

Here, $\tilde{\boldsymbol{R}}_{j+1/2}$ is a matrix of scaled right eigenvectors of the flux Jacobian matrix $\boldsymbol{J}$ evaluated at the average state $\boldsymbol{u}_{j+1/2} = (\boldsymbol{u}_j + \boldsymbol{u}_{j+1})/2$ such that

$$\boldsymbol{u}_{\boldsymbol{v}} = \tilde{\boldsymbol{R}}\tilde{\boldsymbol{R}}^{\mathrm{T}} \tag{3.10}$$

and $\tilde{\boldsymbol{\Lambda}}_{j+1/2}$ is the Roe-type diagonal matrix $\tilde{\boldsymbol{\Lambda}} := \operatorname{diag}(|\lambda_1|, |\lambda_2|, |\lambda_3|, |\lambda_4|, |\lambda_5|)$, where $\lambda_1, \dots, \lambda_5$ are the eigenvalues of $\boldsymbol{J}(\boldsymbol{u}_{j+1/2})$. The flux (3.9) is entropy stable provided that the following sign stability condition, termed *sign property* [9], is satisfied:

$$\operatorname{sgn}\bigl(\langle\langle \boldsymbol{w}\rangle\rangle_{j+1/2}\bigr) = \operatorname{sgn}\bigl([\![\boldsymbol{w}]\!]_{j+1/2}\bigr), \quad \text{where} \quad \langle\langle \boldsymbol{w}\rangle\rangle_{j+1/2} = \boldsymbol{w}^+_{j+1/2} - \boldsymbol{w}^-_{j+1/2},$$

and $\boldsymbol{w}^-_{j+1/2}$ and $\boldsymbol{w}^+_{j+1/2}$ denote the respective left and right limit values of the scaled entropy variables

$$\boldsymbol{w} := \tilde{\boldsymbol{R}}^{\mathrm{T}}_{j+1/2}\boldsymbol{v}$$

at the interface $x_{j+1/2}$. It is well known that k-th order ENO reconstructions satisfy the sign property [10] but arbitrary high order WENO do not. However, Pandey and Dubey [24] recently proposed a procedure to transform any existing high-order reconstruction into a sign stable reconstruction. Irrespective of the reconstruction procedure to be used, the role of the scaled eigenvectors $\tilde{\boldsymbol{R}}_{j+1/2}$ is crucial to obtain the diffusion matrix. The existence of such matrix is proved in [2, Theorem 4]. However, an explicit expression for $\tilde{\boldsymbol{R}}$ is quite complicated for the model under study. The following result shows how to construct the diffusion operator in (3.9) without computing the scaled matrix explicitly. For simplicity of notation, we drop the subscript $j + 1/2$.

Theorem 3.3. *For the augmented (A, U) blood flow model (2.1) the diffusion term in (3.9) can be written as*

$$\boldsymbol{D}\langle\langle \boldsymbol{v}\rangle\rangle = \left(-\alpha|\lambda_1|\langle\langle w_1\rangle\rangle + \beta|\lambda_5|\langle\langle w_5\rangle\rangle, \frac{c}{A}\bigl(\alpha|\lambda_1|\langle\langle w_1\rangle\rangle + \beta|\lambda_5|\langle\langle w_5\rangle\rangle\bigr), 0, 0, 0\right)^{\mathrm{T}}, \tag{3.11}$$

where

$$\alpha := \left(\frac{A}{2c(c-U)}\right)^{1/2}, \quad \beta := \left(\frac{A}{2c(c+U)}\right)^{1/2}, \quad w_1 := \alpha\left(-v_1 + \frac{c}{A}v_2\right), \quad w_5 := \beta\left(v_1 + \frac{c}{A}v_2\right). \tag{3.12}$$

Here v_1 and v_2 are the first two components of the entropy variables and w_1 and w_5 are the corresponding components of the scaled entropy variables.

Proof. The main idea of the proof is to calculate explicitly only some relevant entries of $\tilde{\boldsymbol{R}}$. The eigenscaling theorem [2, Theorem 4] states that the scaled eigenvector matrix $\tilde{\boldsymbol{R}}$ such that $\boldsymbol{u_v}$ satisfies (3.10) is given by

$$\tilde{\boldsymbol{R}} = \boldsymbol{R}\boldsymbol{T}, \tag{3.13}$$

where $\boldsymbol{T}$ is the square root of the symmetric positive matrix $\boldsymbol{Y} \coloneqq \boldsymbol{R}^{-1}\boldsymbol{u_v}\boldsymbol{R}^{-\mathrm{T}}$. Since expressions for $\boldsymbol{R}^{-1}$ and $\boldsymbol{u_v}$ are very involved, we calculate $\boldsymbol{Y}^{-1} = \boldsymbol{R}^{\mathrm{T}}\boldsymbol{v_u}\boldsymbol{R}$ which is easy to compute by using (3.5) and the matrix $\boldsymbol{R}$ whose columns are given by (2.6). First, the Jacobian $\boldsymbol{v_u}$ of the mapping $\boldsymbol{u} \mapsto \boldsymbol{v}$ is given by

$$\boldsymbol{v_u} = \begin{bmatrix} c^2/A & U & \phi/\rho & K\phi_{A_0}/\rho & 1/\rho \\ U & A & 0 & 0 & 0 \\ \phi/\rho & 0 & h_1''(K) & \Phi_{A_0}/\rho & 0 \\ K\phi_{A_0}/\rho & 0 & \Phi_{A_0}/\rho & K\phi_{A_0A_0}/\rho + h_2''(A_0) & 0 \\ 1/\rho & 0 & 0 & 0 & h_3''(P_{\mathrm{e}}) \end{bmatrix}.$$

Then

$$\boldsymbol{Y}^{-1} = \boldsymbol{R}^{\mathrm{T}}\boldsymbol{v_u}\boldsymbol{R} = \operatorname{blockdiag}\left(2c\frac{c-U}{A}, \boldsymbol{Y}_{3\times 3}, 2c\frac{c+U}{A}\right),$$

where

$$\boldsymbol{Y}_{3\times 3} \coloneqq \begin{bmatrix} \dfrac{c^2-U^2}{A}\left(\dfrac{c^2-U^2}{A}\rho h_3'' - 1\right) & \rho\phi h_3''\dfrac{c^2-U^2}{A} & \rho K\phi_{A_0}h_3''\dfrac{c^2-U^2}{A} \\ K\phi_{A_0}h_3''\dfrac{c^2-U^2}{A} & h_1'' + \phi^2 h_3'' & \dfrac{\Phi_{A_0}}{\rho} + \phi K\phi_{A_0}h_3'' \\ \rho K\phi_{A_0}h_3''\dfrac{c^2-U^2}{A} & \dfrac{\Phi_{A_0}}{\rho} + \phi K\phi_{A_0}h_3'' & \dfrac{K\Phi_{A_0A_0}}{\rho} + h_2'' + K^2\phi_{A_0}^2 h_3'' \end{bmatrix}.$$

Therefore

$$\boldsymbol{Y} = \operatorname{blockdiag}\left(\frac{A}{2c(c-U)}, \boldsymbol{Y}_{3\times 3}^{-1}, \frac{A}{2c(c+U)}\right).$$

From this it follows that

$$\boldsymbol{T} = \boldsymbol{Y}^{1/2} = \operatorname{blockdiag}\bigl(\alpha, \boldsymbol{Y}_{3\times 3}^{-1/2}, \beta\bigr),$$

where α and β are given by (3.12). (It is worth pointing out that neither $\boldsymbol{Y}_{3\times 3}^{-1}$ nor $\boldsymbol{Y}_{3\times 3}^{-1/2}$ need to be calculated explicitly, as we will see.) Using (3.13) we may rewrite the scaled matrix as

$$\tilde{\boldsymbol{R}} = \boldsymbol{R}\boldsymbol{T} = \begin{bmatrix} -\alpha & * & * & * & \beta \\ \alpha c/A & * & * & * & \beta c/A \\ 0 & * & * & * & * \\ 0 & * & * & * & 0 \\ 0 & * & * & * & 0 \end{bmatrix}, \tag{3.14}$$

where any unimportant entry is marked by $*$. Thus, the scaled entropy variables can be written as

$$\boldsymbol{w} = \tilde{\boldsymbol{R}}\boldsymbol{v} = \left(\alpha\left(-v_1 + \frac{c}{A}v_2\right), *, *, *, \beta\left(v_1 + \frac{c}{A}v_2\right)\right)^{\mathrm{T}},$$

where v_i denotes the i-th component of the entropy variables $\boldsymbol{v}$. Since $\tilde{\boldsymbol{\Lambda}} = \operatorname{diag}(|\lambda_1|, 0, 0, 0, |\lambda_5|)$, the product of the eigenvalue matrix $\tilde{\boldsymbol{\Lambda}}$ and the jumps in reconstructed values $\langle\!\langle \boldsymbol{w} \rangle\!\rangle$ simplifies to

$$\tilde{\boldsymbol{\Lambda}}\langle\!\langle \boldsymbol{w} \rangle\!\rangle = \bigl(|\lambda_1|\langle\!\langle w_1 \rangle\!\rangle, 0, 0, 0, |\lambda_5|\langle\!\langle w_5 \rangle\!\rangle\bigr)^{\mathrm{T}}.$$

Using this expression along with (3.14) we conclude that $\boldsymbol{D}\langle\langle \boldsymbol{v}\rangle\rangle = \tilde{\boldsymbol{R}}\tilde{\boldsymbol{\Lambda}}\langle\langle \boldsymbol{w}\rangle\rangle$ is given by (3.11), which completes the proof. □

3.5. **Well-balanced property.** The next theorem shows that the scheme (3.1) with numerical flux (3.9) is well-balanced in the sense of preserving a discrete form of the living-man equilibrium (2.7). To shorten notation, we write ϕ_j instead of $\phi(A_j, A_{0,j})$.

Theorem 3.4. *The scheme (3.1) with numerical flux (3.9) given by (3.4), (3.8) and (3.11) is well-balanced for the living-man equilibrium (2.7), this means that given the initial data*

$$A_j U_j = C_1, \quad \frac{U_j^2}{2} + \frac{1}{\rho}(P_{\mathrm{e},j} + K_j\phi_j) = C_2 \quad \text{for all } j \tag{3.15}$$

with constants C_1 and C_2, the solution computed by the scheme satisfies $\mathrm{d}\boldsymbol{u}_j(t)/\mathrm{d}t = 0$ for all j.

Proof. Assumption (3.15) implies that the first two components of the entropy variables described by (3.5) are constant. Therefore, $\langle\langle w_1\rangle\rangle = \langle\langle w_5\rangle\rangle = 0$, and consequently the dissipation term $\boldsymbol{D}\langle\langle \boldsymbol{v}\rangle\rangle$ cancels out by Theorem 3.3. Then

$$\frac{\mathrm{d}\boldsymbol{u}_j(t)}{\mathrm{d}t} = -\frac{1}{\Delta x}\big(\boldsymbol{F}^k_{j+1/2} - \boldsymbol{F}^k_{j-1/2}\big) = -\frac{1}{\Delta x}\big(\tilde{\boldsymbol{F}}^{2p}_{j+1/2} - \tilde{\boldsymbol{F}}^{2p}_{j-1/2}\big).$$

The proof is completed by showing that

$$\tilde{\boldsymbol{F}}^{2p}_{j+1/2} - \tilde{\boldsymbol{F}}^{2p}_{j-1/2} = \boldsymbol{0}.$$

In fact, using the entropy conservative flux $\tilde{\boldsymbol{F}}$ given by (3.4) and (3.8), we obtain

$$\begin{aligned}
\tilde{\boldsymbol{F}}^{2p}_{j+1/2} - \tilde{\boldsymbol{F}}^{2p}_{j-1/2} &= \sum_{i=1}^{p} \gamma_i^p \big(\tilde{\boldsymbol{F}}(\boldsymbol{u}_j, \boldsymbol{u}_{j+i}) - \tilde{\boldsymbol{F}}(\boldsymbol{u}_{j-i}, \boldsymbol{u}_j)\big) \\
&= \frac{1}{2}\sum_{i=1}^{p} \gamma_i^p \begin{pmatrix} A_{j+i}U_{j+i} - A_{j-i}U_{j-i} \\ \dfrac{1}{2}U_{j+i}^2 + \dfrac{P_{\mathrm{e},j+i} + K_{j+i}\phi_{j+i}}{\rho} - \left(\dfrac{1}{2}U_{j-i}^2 + \dfrac{P_{\mathrm{e},j-i} + K_{j-i}\phi_{j-i}}{\rho}\right) \\ 0 \\ 0 \\ 0 \end{pmatrix} \\
&= \frac{1}{2}\sum_{i=1}^{p} \gamma_i^p \begin{pmatrix} C_1 - C_1 \\ C_2 - C_2 \\ 0 \\ 0 \\ 0 \end{pmatrix} = \boldsymbol{0},
\end{aligned}$$

where the penultimate equality is a consequence of the assumption (3.15). □

3.6. **Scheme in final form.** To complete the discretization of (2.1) we use the following third-order strong stability preserving (SSP) Runge-Kutta method [14] for the computation of the vector of approximate solutions $\boldsymbol{u}^{\nu+1}$ associated with $t_{\nu+1} = t_\nu + \Delta t$ from $\boldsymbol{u}^\nu$:

$$\begin{aligned}
\boldsymbol{u}^{(1)} &= \boldsymbol{u}^\nu + \Delta t \boldsymbol{\mathcal{L}}\big(\boldsymbol{u}^\nu\big), \\
\boldsymbol{u}^{(2)} &= \frac{3}{4}\boldsymbol{u}^\nu + \frac{1}{4}\boldsymbol{u}^{(1)} + \frac{1}{4}\Delta t \boldsymbol{\mathcal{L}}\big(\boldsymbol{u}^{(1)}\big), \\
\boldsymbol{u}^{\nu+1} &= \frac{1}{3}\boldsymbol{u}^\nu + \frac{2}{3}\boldsymbol{u}^{(2)} + \frac{2}{3}\Delta t \boldsymbol{\mathcal{L}}\big(\boldsymbol{u}^{(2)}\big),
\end{aligned}$$

TABLE 1. Example 1 (decreasing step): relative L^1 and L^∞ errors for two values of the inlet Shapiro number $S_{\mathrm{h,in}}$ with $N = 100$ cells at time $t = 10\,\mathrm{s}$.

	$S_{\mathrm{h,in}} = 0.01$		$S_{\mathrm{h,in}} = 0.1$	
Variable	L^1-error	L^∞-error	L^1-error	L^∞-error
A	2.4212e-14	5.0032e-14	8.6730e-16	2.8590e-15
U	2.0079e-14	3.8773e-14	6.1531e-16	2.0623e-15
Q	2.3974e-15	8.2533e-15	3.1834e-16	1.3546e-15
E	1.7888e-16	2.0197e-15	6.7735e-16	2.9334e-15

with

$$[\mathcal{L}(\boldsymbol{u})]_j \coloneqq -\frac{1}{\Delta x}\big(\boldsymbol{F}^k_{j+1/2} - \boldsymbol{F}^k_{j-1/2}\big).$$

Here, the kth-order numerical flux is given by

$$\boldsymbol{F}^k_{j+1/2} = \tilde{\boldsymbol{F}}^{2p}_{j+1/2} - \frac{1}{2}\boldsymbol{D}_{j+1/2}\langle\!\langle \boldsymbol{v} \rangle\!\rangle_{j+1/2},$$

where the $2p$th-order ($p = k/2$) entropy conservative flux $\tilde{\boldsymbol{F}}^{2p}_{j+1/2}$ is defined by (3.4) and (3.8) and the diffusion term $\boldsymbol{D}_{j+1/2}\langle\!\langle \boldsymbol{v} \rangle\!\rangle_{j+1/2}$ is defined by (3.11). The reconstruction procedure of scaled entropy variables is carried out using the ENO method which satisfies the sign property. Thus, the scheme is termed as TeCNO-k when this is based on a combination of k-order entropy conservative flux and kth-order dissipation operators [9]. To ensure stability of the method, the time step Δt is computed adaptively for each step ν. More precisely, the solution $\boldsymbol{u}^{\nu+1}$ at $t_{\nu+1} = t_\nu + \Delta t$ is calculated from $\boldsymbol{u}^\nu$ by taking

$$\Delta t = \mathrm{CFL}\frac{\Delta x}{\max_j\{|\lambda_5(\mathbf{u}^\nu_j)|\}},$$

where we choose the CFL number CFL = 0.5.

4. Numerical examples

This section is dedicated to evaluate the performance of the proposed scheme. In particular, we verify the well-balanced property by using smooth and discontinuous configurations of the varying parameters and initial data. All quantities are expressed in the International System of Units (SI) in which the basic units are seconds (s), meters (m) and kilograms (kg). The blood density is taken as $\rho = 1050\,\mathrm{kg/m^3}$ and the tests are run with $N = 100$ uniform cells.

Example 1: decreasing step. In this example, we evaluate the well-balanced property for the case of a decreasing step o decreasing discontinuity which represents an idealized transition of blood flow from a parent to a daughter artery. This example was proposed in [15] by taking only K and A_0 variable. However, we also take P_e variable. In this case the function ϕ given by (1.3) is characterized by the parameters $m = 1/2$ and $n = 0$. Two configurations are considered: a decreasing discontinuity (decreasing step) and a smooth stenosis. In both cases, the initial conditions are determined from the steady-state solution

$$Q_{\mathrm{st}} = A_{\mathrm{in}}U_{\mathrm{in}}, \qquad E_{\mathrm{st}} = \frac{Q^2_{\mathrm{st}}}{2A^2_{\mathrm{out}}} + \frac{1}{\rho}\left(P_\mathrm{e}(L) + K(L)\left(\sqrt{A_{\mathrm{out}}} - \sqrt{A_0(L)}\right)\right),$$

TABLE 2. Example 2 (smooth stenosis): relative L^1 and L^∞ errors for two values of the inlet Shapiro number $S_{\mathrm{h,in}}$ with $N = 100$ cells at time $t = 10$ s.

	$S_{\mathrm{h,in}} = 0.01$		$S_{\mathrm{h,in}} = 0.1$	
Variable	L^1-error	L^∞-error	L^1-error	L^∞-error
A	4.6860e-15	1.4809e-14	1.4120e-15	4.0826e-15
U	7.3150e-16	1.4601e-15	7.1484e-16	3.5139e-15
Q	5.3869e-15	1.6245e-14	1.5172e-15	4.5719e-15
E	1.4526e-15	2.8850e-15	1.2431e-15	2.8011e-15

where the subscripts "in" and "out" represent the values at the inlet (left side) and outlet (right side) of the domain respectively, and $L = 0.1\,\mathrm{m}$ is the length of the artery. The values of A_{in} and A_{out} can be computed from the cross-sectional area at rest and the Shapiro number at the inlet $S_{\mathrm{h,in}}$, namely

$$A_{\mathrm{in}} = A_0(0)(1 + S_{\mathrm{h,in}})^2, \qquad A_{\mathrm{out}} = A_0(L)(1 + S_{\mathrm{h,in}})^2.$$

The Moens-Korteweg velocity at the inlet is given by

$$c_{\mathrm{in}} = \sqrt{\frac{K(0)\sqrt{A_{\mathrm{in}}}}{2\rho\sqrt{\pi}}}.$$

Using the expression (2.5) we may determine the velocity at the inlet as a function of the Shapiro number, i.e.,

$$U_{\mathrm{in}} = S_{\mathrm{h,in}} c_{\mathrm{in}}.$$

The cross-sectional area at rest is $A_0(x) = \pi R_0^2(x)$, where the radius at rest is given by

$$R_0(x) = \begin{cases} R_{\mathrm{in}} & \text{if } x < x_{\mathrm{g}}, \\ R_{\mathrm{in}}(1 - \Delta\mathcal{G}) & \text{if } x \geq x_{\mathrm{g}}, \end{cases}$$

where $R_{\mathrm{in}} = 5 \times 10^{-3}\,\mathrm{m}$, $\Delta\mathcal{G} = 0.1$ and $x_{\mathrm{g}} = L/2$. The arterial wall rigidity $K(x)$ is taken as

$$K(x) = \begin{cases} K_{\mathrm{in}} & \text{if } x < x_{\mathrm{g}}, \\ K_{\mathrm{in}}(1 + \Delta\mathcal{G}) & \text{if } x \geq x_{\mathrm{g}}, \end{cases}$$

where the inlet rigidity is $K_{\mathrm{in}} = 1 \times 10^8\,\mathrm{Pa/m}$. Finally, the external pressure is given by

$$P_{\mathrm{e}}(x) = \begin{cases} P_{\mathrm{e,in}} & \text{if } x < x_{\mathrm{g}}, \\ P_{\mathrm{e,in}}(1 + \Delta\mathcal{G}) & \text{if } x \geq x_{\mathrm{g}}, \end{cases}$$

with $P_{\mathrm{e,in}} = 9999.15\,\mathrm{Pa}$. The L^1 and L^∞ relative errors at final time $t = 10\,\mathrm{s}$ with $N = 100$ mesh points for $S_{\mathrm{h,in}} = 0.01$ and $S_{\mathrm{h,in}} = 0.1$ are presented in Table 1. As it can be seen, the proposed scheme preserves the living-man steady solution in an artery with discontinuous variation.

TABLE 3. Examples 3, 4 and 5 (Riemann problems): initial left and right states.

Left states	A_l	U_l	K_l	$A_{0,\mathrm{l}}$	$P_{\mathrm{e,l}}$
Example 3	6.4136e-4	1.0	58725	6.2706e-4	9999.15
Example 4	2.5082e-4	1.0	58725	1.5677e-4	3999.66
Example 5	3.1e-5	-0.2	33.3333	2.82e-74e-5	66.661
Right states	A_r	U_r	K_r	$A_{0,\mathrm{r}}$	$P_{\mathrm{e,r}}$
Example 3	3.109988e-4	2.06224886	587250	3.1353e-4	78002.20
Example 4	3.2921e-4	0.0	587250	3.1353e-4	0
Example 5	3.1e-5	0.1	1761750	3.2921e-04	66.661

Example 2: smooth stenosis. This test corresponds to an aortic stenosis with a smooth local reduction of the cross-sectional area at rest. The radius at rest, arterial wall rigidity and the external pressure are defined by

$$R_0(x) = \begin{cases} R_{\mathrm{in}} & \text{if } x \in [0, x_1] \cup [x_2, L], \\ R_{\mathrm{in}} \left(1 - \dfrac{\Delta\mathcal{G}}{2}\left(1 + \cos\left(\pi + 2\pi\dfrac{x - x_1}{x_2 - x_1}\right)\right)\right) & \text{if } x \in [x_1, x_2], \end{cases}$$

$$K(x) = \begin{cases} K_{\mathrm{in}} & \text{if } x \in [0, x_1] \cup [x_2, L], \\ K_{\mathrm{in}} \left(1 + \dfrac{\Delta\mathcal{G}}{2}\left(1 + \cos\left(\pi + 2\pi\dfrac{x - x_1}{x_2 - x_1}\right)\right)\right) & \text{if } x \in [x_1, x_2], \end{cases}$$

$$P_\mathrm{e}(x) = \begin{cases} P_{\mathrm{e,in}} & \text{if } x \in [0, x_1] \cup [x_2, L], \\ P_{\mathrm{e,in}} \left(1 + \dfrac{\Delta\mathcal{G}}{2}\left(1 + \cos\left(\pi + 2\pi\dfrac{x - x_1}{x_2 - x_1}\right)\right)\right) & \text{if } x \in [x_1, x_2], \end{cases}$$

where $x_1 = 0.3L$, $x_2 = 0.7L$ and the parameters L, $\Delta\mathcal{G}$, K_{in}, R_{in} and $P_{\mathrm{e,in}}$ are the same as in the previous example. The L^1 and L^∞ relative errors are shown in Table 2, where it can be observed that the non-trivial steady state solution is also preserved in an artery with smooth variation.

Examples 3 to 5: Riemann problems. In Examples 3 to 5, taken from [26], we consider Riemann problems, that is initial data with a single discontinuity, namely an initial datum $\boldsymbol{u}(x,0)$ given by

$$\boldsymbol{u}(x,0) = \begin{cases} \boldsymbol{u}_\mathrm{l} = (A_\mathrm{l}, U_\mathrm{l}, K_\mathrm{l}, A_{0,\mathrm{l}}, P_{\mathrm{e,l}})^\mathrm{T} & \text{if } x < x_\mathrm{g} \\ \boldsymbol{u}_\mathrm{r} = (A_\mathrm{r}, U_\mathrm{r}, K_\mathrm{r}, A_{0,\mathrm{r}}, P_{\mathrm{e,r}})^\mathrm{T} & \text{if } x \geq x_\mathrm{g}, \end{cases} \tag{4.1}$$

where the left and right states are given in Table 3. In all of the examples, free boundary conditions are taken.

In Example 3, we consider a small perturbation of A for a discontinuous stationary solution. To be more precise, the perturbed initial conditions are given by

$$\boldsymbol{u}_{\mathrm{pert}}(x,0) = \boldsymbol{u}(x,0) + \boldsymbol{\delta}(x),$$

where $\boldsymbol{\delta}(x) \coloneqq (0.00001 \exp(-20000(x-0.05)^2), 0, 0, 0, 0)^\mathrm{T}$ and $\boldsymbol{u}(x,0)$ is the stationary solution (4.1) with left and right states given in Table 3. Here the initial discontinuity is located at $x_\mathrm{g} = 0.5L$, where $L = 0.2\,\mathrm{m}$ is the length of the vein. Tube law exponential coefficients are $m = 10$ and $n = -1.5$. Comparisons of the numerical solutions and the initial conditions for variables A and U

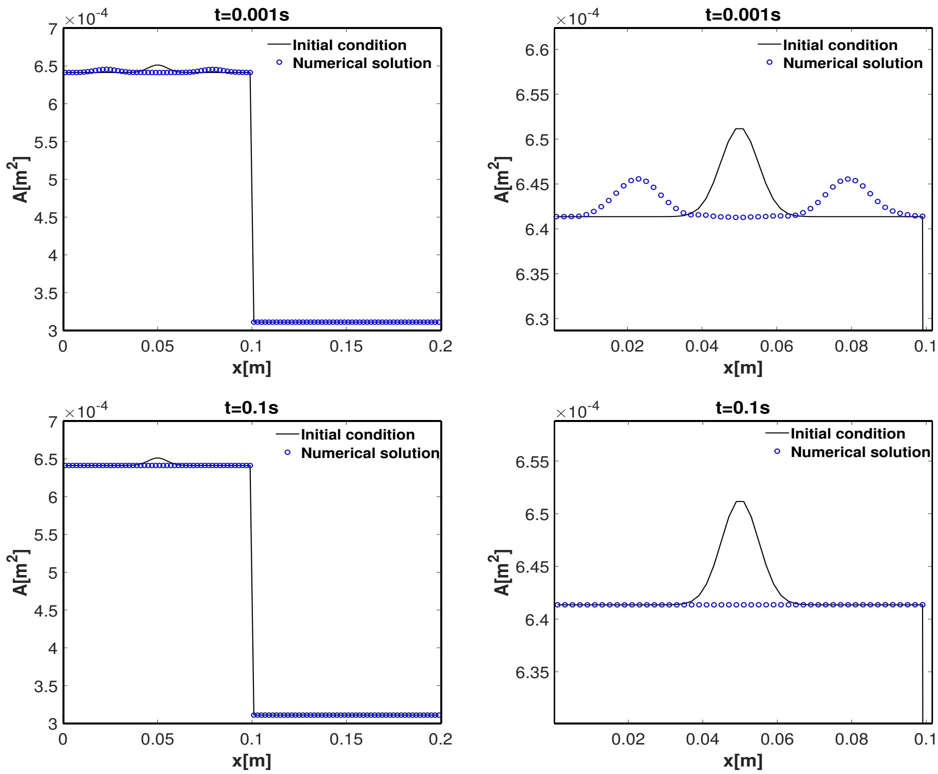

FIGURE 1. Example 3 (Riemann problem): comparison between the initial condition and the numerical solution for the variable A at two times (left column) and the corresponding enlarged views (right column).

are presented in Figures 1 and 2, respectively. As one can see, once the initial perturbation leaves the domain, the proposed scheme accurately recovers the stationary solution.

Examples 4 and 5 correspond to Riemann problems labeled as RP-1 and RP-2 in [26]. The left and right states are listed in Table 3. For Example 4, the test RP-1, we take $L = 0.2\,\mathrm{m}$, $x_{\mathrm{g}} = 0.3L$, $m = 0.5$, and $n = 0$. In this case the solution consists of two shocks moving in opposite directions and that are separated by a stationary contact discontinuity in an artery. For Example 5 (the test RP-2), we have $L = 0.5\,\mathrm{m}$, $x_{\mathrm{g}} = 0.5L$, $m = 10$, and $n = -1.5$. In this case, the solution consists of two rarefactions traveling in opposite directions separated by a stationary contact discontinuity in a vein. Numerical and exact solutions are shown in Figures 3 and 4 including 3D graphics with time evolution. In order to verify that the scheme is entropy stable at the discrete level we compute the relative change in total entropy for $t = t_\nu = \nu \Delta t$ as

$$\frac{\eta(t_\nu) - \eta(0)}{\eta(0)}, \quad \text{where} \quad \eta(t_\nu) := \Delta x \sum_{j=1}^{N} \eta\bigl(\boldsymbol{u}_j(t_\nu)\bigr).$$

We show in Figure 5 the relative entropy for Examples 4 and 5 taking into account that solutions for these tests develop discontinuities. As expected, the entropy decreases over time.

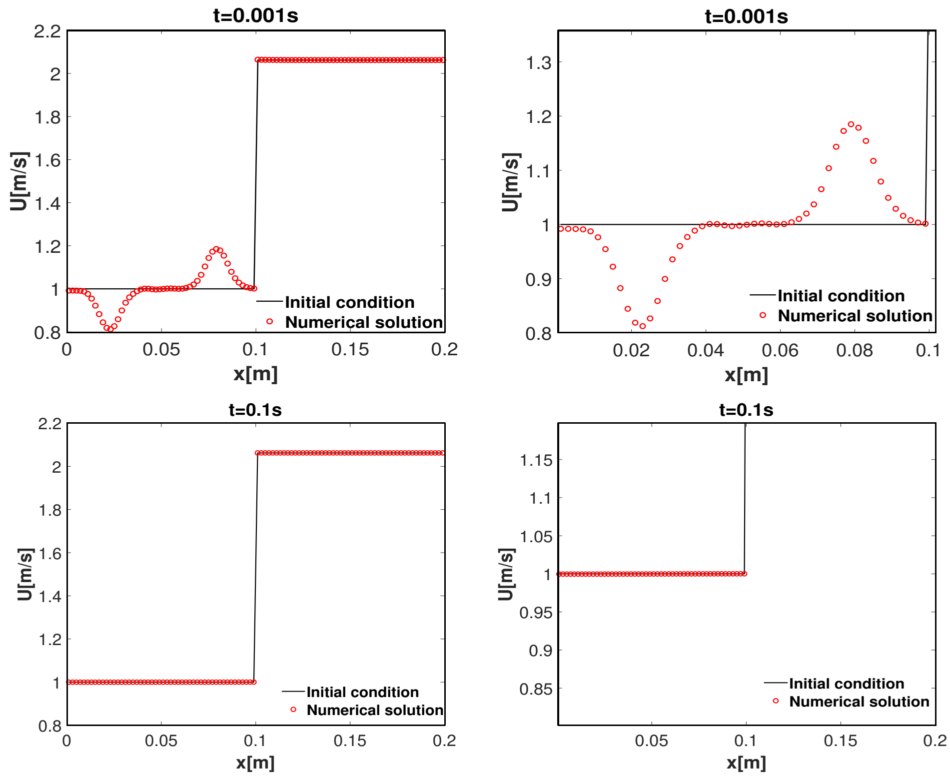

FIGURE 2. Example 3 (Riemann problem): comparison between the initial condition and the numerical solution for the variable U at two times (left column) and the corresponding enlarged views (right column).

5. CONCLUSIONS

In this article, we have designed a well-balanced and entropy stable finite volume scheme, based on the framework of [9], for an augmented one-dimensional blood flow model which is obtained by taking the arterial wall rigidity, the cross-sectional area at rest and the external pressure as unknowns. We gave demonstrated that this model preserves the living-man equilibrium (2.7), which includes as a special case the man-at-eternal-rest steady state (2.8). Furthermore, and in a fashion similar to [5, 9, 34], numerical diffusion in terms of entropy variables was added to the EC scheme to obtain an entropy stable scheme. Numerical tests demonstrate that the proposed scheme preserves the steady state and gives good resolution for discontinuous solutions. Notice that satisfaction of the well-balanced property arises in a natural way from the design of the EC flux (3.4), with no need to discretize the source terms $(1/\rho)P_x$ (see (1.1), (1.2)) as a consequence of the augmented formulation. This approach provides an alternative to handling the source terms by hydrostatic reconstruction, as was done, for instance, in [15, 17, 26], which is based on specific flux correction terms to achieve the well-balanced property.

Furthermore, according to what we emphasize at the beginning of the proof of Theorem 3.4 (and similarly to what we commented in our previous work [5]), the diffusive correction introduced in Section 3.4 is zero whenever the initial data are chosen by (3.15) so the well-balanced property is not affected by the diffusive correction. We also mention that Wand et al. [37] proved the well-balanced property for the (A, Q) model for all linear schemes (such that are based on approximating all spatial

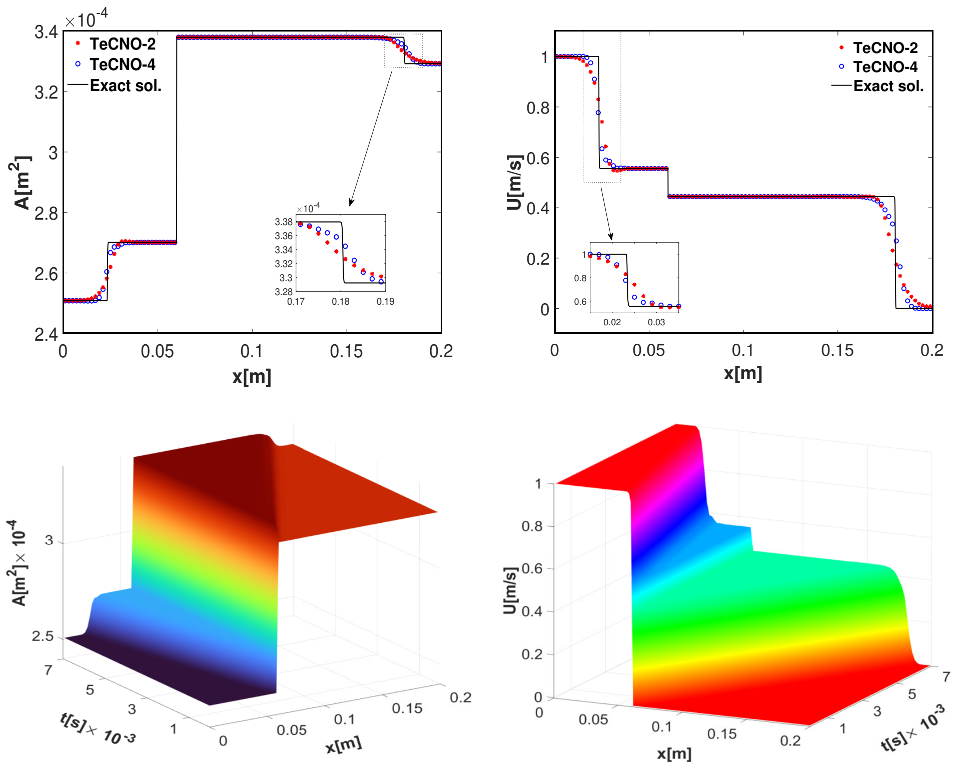

FIGURE 3. Example 4 (Riemann problem RP-1): comparison between numerical and exact solution (first row) at simulated time $t = 0.007$ s and 3D-graphics with time evolution (second row).

derivatives by a linear finite difference operator). Within our approach, the construction of EC fluxes produces a linear scheme, but the construction of diffusive corrections by ENO reconstruction introduces nonlinearity, so the well-balanced property of our scheme does not follow from the treatment in [37].

Acknowledgements

RB is supported by ANID (Chile) through projects Fondecyt 1210610; Anillo ANID/ACT210030; Centro de Modelamiento Matemático (CMM), project FB210005 of BASAL funds for Centers of Excellence; and CRHIAM, projects ANID/FONDAP/15130015 and ANID/FONDAP/1523A0001. CV wishes to thank the Centro de Investigación en Ingeniería Matemática (CI^{2}MA), where part of the paper was written, for the invitation and hospitality.

References

[1] J. Alastruey, A. W. Khir, K. S. Matthys, P. Segers, S. J. Sherwin, P. R. Verdonck, K. H. Parker, J. Peiró, Pulse wave propagation in a model human arterial network: Assessment of 1-D viscoelastic simulations against *in vitro* measurements, J. Biomech. 44 (2011) 2250–2258.

[2] T. J. Barth, Numerical Methods for Gas-Dynamics Systems on Unstructured Meshes: An Introduction to Recent Developments in Theory and Numerics of Conservation Laws, in D. Kröner, M. Ohlberger, and C. Rohde (eds.), Lecture Notes in Comput. Sci. Engrg., Springer, Berlin, vol. **5** (1999) 195–285.

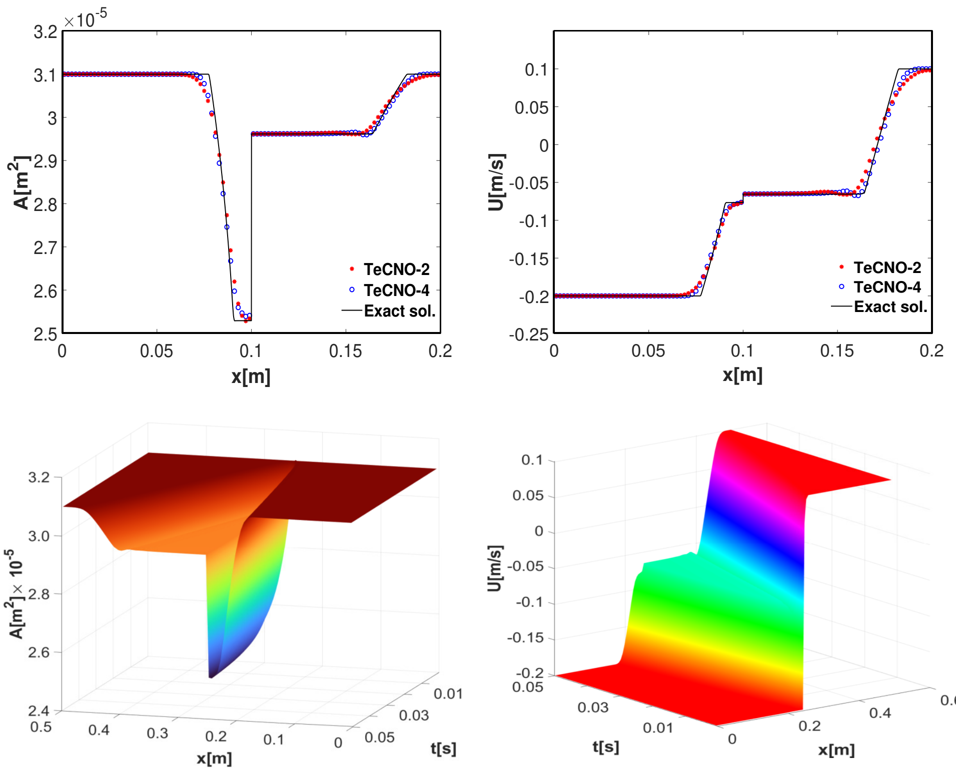

FIGURE 4. Example 5 (Riemann problem RP-2): comparison between numerical and exact solution (first row) at simulated time $t = 0.05\,\mathrm{s}$ and 3D-graphics with time evolution (second row).

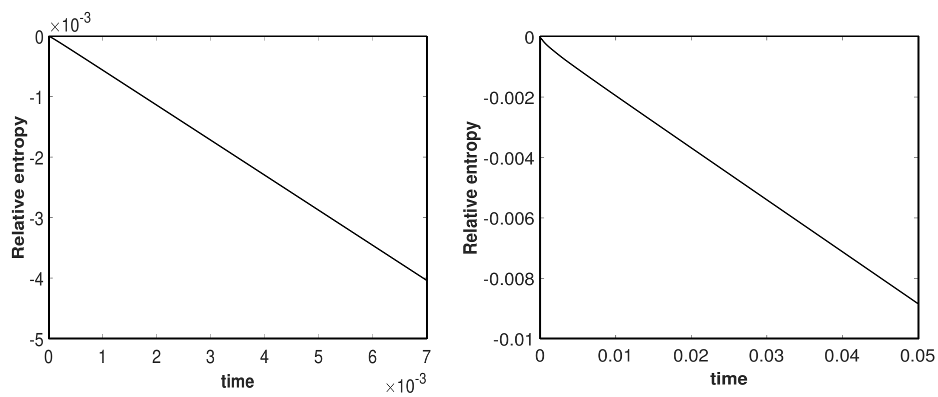

FIGURE 5. Examples 4 and 5 (Riemann problems RP-1 and RP-2): relative entropy for RP-1 (left) and RP-2 (right). It can be observed that this quantity decrease over time.

[3] E. Boileau, P. Nithiarasu, P. J. Blanco, L. O. Müller, F. E. Fossan, L. R. Hellevik, W. P. Donders, W. Huberts, M. Willemet, J. Alastruey, A benchmark study of numerical schemes for one-dimensional arterial blood flow modelling, Int. J. Numer. Meth. Biomed. Engng. 31 (2015) 1–33.

[4] J. Britton, Y. Xing, Well-balanced discontinuous Galerkin methods for the one-dimensional blood flow through arteries model with man-at-eternal-rest and living-man equilibria, Comput. Fluids 203 (2020) 104493.
[5] R. Bürger, S. Valbuena, C. Vega, A well-balanced and entropy stable scheme for a reduced blood flow model, Numer. Meth. Part. Differ. Equ. 39 (2023) 2491–2509.
[6] S. Chu, A. Kurganov, Flux globalization based well-balanced central-upwind scheme for one-dimensional blood flow models, Calcolo 60 (2023) 101007.
[7] O. Delestre, P. Y. Lagrée, 'Well-balanced' finite volume scheme for blood flow simulation, Int. J. Numer. Methods Fluids 72 (2013) 177–205.
[8] L. Euler, Principia pro motu sanguinis per arterias determinando, Opera posthuma vol. 2 (1862) 814—823.
[9] U. S. Fjordholm, S. Mishra, E. Tadmor, Arbitrary high-order essentially non-oscillatory entropy stable schemes for systems of conservation laws, SIAM J. Numer. Anal. 50 (2012) 544–573.
[10] U. S. Fjordholm, S. Mishra, E. Tadmor, ENO reconstruction and ENO interpolation are stable, Found. Comput. Math. 13 (2013) 139–159.
[11] L. Formaggia, J. F. Gerbeau, F. Nobile, A. Quarteroni, On the coupling of 3D and 1D Navier-Stokes equations for flow problems in compliant vessels, Comput. Methods Appl. Mech. Engrg. 191 (2001) 561–582.
[12] L. Formaggia, D. Lamponi, A. Quarteroni, One-dimensional models for blood flow in arteries, J. Eng. Math. 47 (2003) 251-–276.
[13] J. M. Fullana, S. Zaleski, A branched one-dimensional model of vessel networks, J. Fluid Mech. 621 (2009) 183-–204.
[14] S. Gottlieb, C.-W. Shu, E. Tadmor, Strong stability-preserving high-order time discretization methods, SIAM Rev. 43 (2001) 89–112.
[15] A. R. Ghigo, O. Delestre, J.-M. Fullana, P. Y. Lagrée, Low-Shapiro hydrostatic reconstruction technique for blood flow simulation in large arteries with varying geometrical and mechanical properties, J. Comput. Phys. 331 (2017) 108–136.
[16] P. G. LeFloch, J. M. Mercier, C. Rohde, Fully discrete entropy conservative schemes of arbitrary order, SIAM J. Numer. Anal. 40 (2002) 1968–1992.
[17] G. Li, O. Delestre, Y. Yuan, Well-balanced discontinuous Galerkin method and finite volume WENO scheme based on hydrostatic reconstruction for blood flow model in arteries, Int. J. Numer. Methods Fluids 86 (2020) 491–508.
[18] M. Mock, Systems of conservation laws of mixed type, J. Differ. Equ. 37 (1980) 70-78.
[19] L. O. Müller, C. Parés, E. F. Toro, Well-balanced high-order numerical schemes for one-dimensional blood flow in vessels with varying mechanical properties, J. Comput. Phys. 242 (2013) 53–85.
[20] L. O. Müller, E. F. Toro, Well-balanced high-order solver for blood flow in networks of vessels with variable properties, Int. Numer. Meth. Biomed. Engng. 29 (2013) 1388–1411.
[21] J. P. Mynard, P. Nithiarasu, A 1D arterial blood flow model incorporating ventricular pressure, aortic valve and regional coronary flow using the locally conservative Galerkin (LCG) method, Commun. Numer. Methods Engrg. 24 (2008) 367–417.
[22] M. S. Olufsen, C. S. Peskin, W. Y. Kim, E. M. Pedersen, A. Nadim, J. Larsen, Numerical simulation and experimental validation of blood flow in arteries with structure-tree outflow conditions, Ann. Biomed. Eng. 28 (2000) 1281–1299.
[23] M. U. Qureshi, G. D. A. Vaughan, C. Sainsbury, M. Johnson, C. S. Peskin, M. S. Olufsen, N. A. Hill, Numerical simulation of blood flow and pressure drop in the pulmonary arterial and venous circulation, Biomech. Model Mechanobiol. 13 (2014) 1137–1154.
[24] P. K. Pandey, R. K. Dubey, Sign stable arbitrary high order reconstruction for constructing non-oscillatory entropy stable schemes, Appl. Math. Comput. 454 (2023) 128099.
[25] R. M. Padmos, T. I. Józsa, W. K. El-Bouri, P. R. Konduri, S. J. Payne, A. G. Hoekstra, Coupling one-dimensional arterial blood flow to thre-dimensional tissue perfusion models for in *in silico* trials of acute ischaemic stroke, Interface Focus 11 (2020) 20190125.
[26] E. Pimentel-García, L. O. Müller, E. F. Toro, C. Parés, High-order fully well-balanced numerical methods for one-dimensional blood flow with discontinuous properties, J. Comput. Phys. 475 (2023) 111869.
[27] F. Piccioli, G. Bertaglia, A. Valiani V. Caleffi, Modeling blood flow in networks of viscoelastic vessels with the 1-D augmented fluid-structure interaction system, J. Comput. Phys. 464 (2022) 111364.
[28] C. Puelz, S. Čanić, B. Rivière, C. G. Rusin, Comparison of reduced models for blood flow using Runge-Kutta discontinuous Galerkin methods, Appl. Numer. Math. 115 (2017) 114–141.

[29] C. A. Rosales-Alcantar, G. Hernández-Dueñas, A new two-dimensional blood flow model with arbitrary cross sections, ESAIM: Math. Model. Numer. Anal. 57 (2023) 1657–1690.
[30] W. Sheng, Q. Zheng, Y. Zheng, The Riemann problem for a blood flow model in arteries, Commun. Comput. Phys. 27 (2020) 227–250.
[31] S. J. Sherwin, V. Franke, J. Peiró, K. Parker, One-dimensional modelling of a vascular network in space–time variables, J. Eng. Math. 47 (2003) 217-–250.
[32] A. Spilimbergo, E. F. Toro, L. O. Müller, One-dimensional blood flow with discontinuous properties and transport: Mathematical analysis and numerical schemes, Commun. Comput. Phys. 29 (2021) 649–697.
[33] E. Tadmor, The numerical viscosity of entropy stable schemes for systems of conservation laws, I. Math. Comp. 49 (1987) 91–103.
[34] E. Tadmor, Entropy stability theory for difference approximations of nonlinear conservation laws and related time-dependent problems, Acta Numer. 12 (2003), 451–512.
[35] E. F. Toro, A. Siviglia, Flow in collapsible tubes with discontinuous mechanical properties: Mathematical model and exact solutions, Commun. Comput. Phys. 13 (2013) 361–385.
[36] X. Wang, J. M. Fullana, P. Y. Lagrée, Verification and comparison of four numerical schemes for 1D viscoelastic blood flow model, Comput. Methods Biomech. Biomed. 18 (2015) 1704–1725.
[37] Z. Wang, G. Li, O. Delestre, Well-balanced finite difference weighted essentially non-oscillatory schemes for the blood flow model, Int. J. Numer. Methods Fluids 82 (2016) 607–622.

Centro de Investigación en Ingeniería Matemática (CI²MA)

PRE-PUBLICACIONES 2024 - 2025

2024-19 Isaac Bermudez, Jessika Camaño, Ricardo Oyarzúa, Manuel Solano: *A conforming mixed finite element method for a coupled Navier–Stokes/transport system modelling reverse osmosis processes*

2024-20 Ana Alonso-Rodriguez, Jessika Camaño, Ricardo Oyarzúa: *Analysis of a FEM with exactly divergence-free magnetic field for the stationary MHD problem*

2024-21 Tomás Barrios, Edwin Behrens, Rommel Bustinza: *On the approximation of the Lamé equations considering nonhomogeneous Dirichlet boundary condition: A new approach*

2024-22 Anahi Gajardo, Victor H. Lutfalla, Michaël Rao: *Ants on the highway*

2024-23 Julio Aracena, Luis Cabrera-Crot, Adrien Richard, Lilian Salinas: *Dynamically equivalent disjunctive networks*

2024-24 Julio Aracena, Raúl Astete-Elguin: *K-independent boolean networks*

2024-25 Sergio Carrasco, Sergio Caucao, Gabriel N. Gatica: *A twofold perturbed saddle point-based fully mixed finite element method for the coupled Brinkman Forchheimer Darcy problem*

2024-26 Juan Barajas-Calonge, Raimund Bürger, Pep Mulet, Luis M. Villada: *Invariant-region-preserving central WENO schemes for one-dimensional multispecies kinematic flow models*

2024-27 Raimund Bürger, Claudio Muñoz, Sebastián Tapia: *Interaction of jamitons in second-order macroscopic traffic models*

2025-01 Boumediene Chentouf, Sabeur Mansouri, Mauricio Sepúlveda, Rodrigo Véjar: *Theoretical and numerical results for the exponential stability of the rotating disk-beam system with a boundary infinite memory of type angular velocity*

2025-02 Julio Aracena, Arturo Zapata-Cortés: *Hamiltonian dynamics of boolean networks*

2025-03 Raimund Bürger, Andrés Guerra, Carlos A. Vega: *An entropy stable and well-balanced scheme for an augmented blood flow model with variable geometrical and mechanical properties*

Para obtener copias de las Pre-Publicaciones, escribir o llamar a: Director, Centro de Investigación en Ingeniería Matemática, Universidad de Concepción, Casilla 160-C, Concepción, Chile, Tel.: 41-2661324, o bien, visitar la página web del centro: http://www.ci2ma.udec.cl

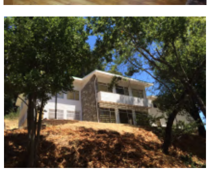

CENTRO DE INVESTIGACIÓN EN
INGENIERÍA MATEMÁTICA (CI^{2}MA)
Universidad de Concepción

Casilla 160-C, Concepción, Chile
Tel.: 56-41-2661324/2661554/2661316
http://www.ci2ma.udec.cl